Production of K Mesons in Three-Body States in Proton-Proton Interactions at 6 BeV/c*

W. CHINOWSKY, R. R. KINSEY, S. L. KLEIN, M. MANDELKERN, AND J. SCHULTZ†
Lawrence Radiation Laboratory, University of California, Berkeley, California

AND

F. MARTIN, M. L. PERL, AND T. H. TAN
Stanford Linear Accelerator Center, Stanford University, Stanford, California

(Received 31 August 1967)

Analysis of 9700 events, containing at least one observed neutral or charged decay, produced by 6-BeV/c protons in the LRL 72-in. liquid-hydrogen bubble chamber has yielded 1746 examples of the reaction proton+proton → hyperon+K meson+nucleon. Production cross sections for these three-body reactions are as follows:

$$\sigma(\Lambda K^+p)=54_{-5}^{+3}\ \mu\text{b},\quad \sigma(\Sigma^0K^+p)=17_{-2}^{+4}\ \mu\text{b},\quad \sigma(\Sigma^+K^0p)=26\pm4\ \mu\text{b},\quad \sigma(\Sigma^+K^+n)=57\pm7\ \mu\text{b}.$$

Strong N^* production is observed in all channels. In particular, one or more $T=\frac{1}{2}$ resonant states with mass near 1700 MeV/c^2, decaying into ΛK^+, and a $T=\frac{3}{2}$ resonance with mass 1920 MeV/c^2, decaying into Σ^+K^+, are produced. In all cases the data are consistent with a production process dominated by a single-pion-exchange mechanism. No evidence is found for a dibaryon state in either the Λ-proton or Σ-nucleon system.

I. INTRODUCTION

IT has been well established that the strong interactions of mesons with nucleons, and of mesons with mesons, are invariant to a good approximation under the operations of the group $SU(3)$. As first discussed by Oakes,[1] it is straightforward to extend the application of this symmetry requirement to the baryon-baryon interaction and to classify multibaryon states as members of irreducible representations of this group. Since the nucleon is a member of an octet, it follows that the deuteron, a system of hypercharge two and isotopic spin zero, belongs to a $\overline{\mathbf{10}}$ representation, and the virtual isotopic triplet state of the deuteron occurs in a **27** representation. The validity of this classification and thus of the relevance of $SU(3)$ symmetry to the nuclear-binding interactions would be most directly established by the discovery of other members of the representations as bound states or resonant interactions of hyperon and nucleon or hyperon and hyperon. Investigations of hyperon-nucleon interactions, both in elastic scattering[2] and final-state interactions[3] of particles produced in nucleon-nucleon collisions have not as yet yielded any conclusive evidence for a resonance in the hyperon-nucleon system. The only indication of such a resonance is the reported enhancement in the Λ-p mass spectrum near minimum Λ-p mass in small-momentum-transfer p-p collisions.[3] To search more intensively for such baryon-baryon states and to reveal more general details of nucleon-nucleon reaction mechanisms, an extensive study of proton interactions in the LRL 72-in. liquid-hydrogen bubble chamber was undertaken. We report here results on the observed characteristics of hyperon production in three-body final states via the channels

$$pp\rightarrow \Lambda K^+p \quad \text{(a)},$$
$$\Sigma^0K^+p \quad \text{(b)},$$
$$\Sigma^+K^0p \quad \text{(c)},$$
$$\Sigma^+K^+n \quad \text{(d)}.$$

The states produced in these reactions would appear to be most suitable for elucidation of final-state hyperon-nucleon interactions, whose effects might be obscured in states including pions by the presence of Y^*, N^*, and K^* resonances. The data reported result from analysis of approximately 500 000 photographs, taken in two separate running periods, of interactions of protons in a beam averaging ten particles per pulse. The incident momentum was 6.10±0.02 BeV/c during the first running period and 6.00±0.02 BeV/c during the second.

II. EXPERIMENTAL PROCEDURE

Protons, produced in a target $\frac{3}{8}$ in. high, $\frac{1}{4}$ in. wide, and $\frac{1}{2}$ in. long at 7° to the direction of the external proton beam of the bevatron, were transported to the bubble chamber using the arrangement shown schematically in Fig. 1. The optical elements determining the focal

* Work done under the auspices of the U. S. Atomic Energy Commission.

† Present address: University of California, Irvine, Calif.

[1] R. J. Oakes, Phys. Rev. **131**, 2239 (1963).

[2] B. Sechi-Zorn, R. A. Burnstein, T. B. Day, B. Kehoe, and G. A. Snow, Phys. Rev. Letters **13**, 282 (1964); L. Piekenbrock and F. Oppenheimer, *ibid.* **12**, 625 (1964); J. Schultz, R. Kinsey, W. Chinowsky, and N. Rybicki, Bull. Am. Phys. Soc. **10**, 529 (1965); R. Englemann, H. Filthuth, V. Hepp, and E. Kluge, Phys. Letters **21**, 587 (1966); H. G. Dosch, R. Englemann, H. Filthuth, V. Hepp, and E. Kluge, *ibid.* **21**, 236 (1966); R. A. Burnstein, University of Maryland Technical Report No. 469, 1965 (unpublished).

[3] A. C. Melissinos, N. W. Reay, J. T. Reed, T. Yamanouchi, E. Sacharidis, S. J. Lindenbaum, S. Ozaki, and L. C. L. Yaun, Phys. Rev. Letters **14**, 604 (1965); P. A. Piroué, Phys. Letters **11**, 164 (1964); W. J. Hogan, P. F. Kuny, A. Lemonick, P. A. Piroué, and A. J. S. Smith, Bull. Am. Phys. Soc. **12**, 517 (1965); W. A. Wenzel (private communication); G. Alexander, O. Benary, B. Reuter, A. Shapiro, E. Simopoulou, and G. Yekutieli, Phys. Rev. Letters **15**, 207 (1965).

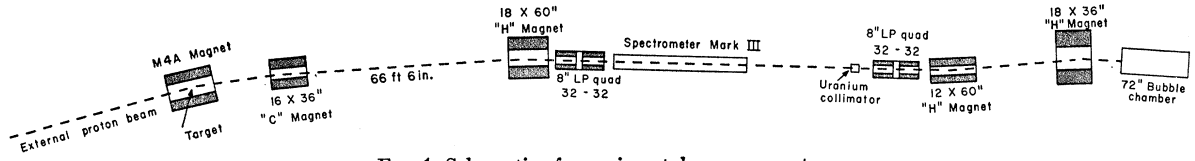

FIG. 1. Schematic of experimental arrangement.

properties of the beam at the uranium collimator were the first quadrupole pair, which yielded vertical magnification 0.5 and unit horizontal magnification, and the two bending magnets producing a dispersion of ~ 1 in. per 1% $\Delta P/P$. Momentum definition of $\pm 0.15\%$ was provided by the slit, of dimensions $\frac{1}{2}$ in. vertically and $\frac{1}{4}$ in. horizontally, in the 12-in.-thick uranium collimator. To allow multiple operation of external beam foci, targeting techniques were needed which would minimize interference with external beam optics, since the target could not conveniently be located at an image position. In the first running period, during which about half the photographs were taken, a polyethylene target was fixed in position in the beam. During the remainder of the run a copper target was fixed at a distance of $\frac{3}{4}$ in. from the normal external beam position and the beam deflected onto it by a magnet[4] pulsed on for approximately 500 μsec. In this way, independent intensity control was achieved with the remainder of the beam available for other experiments. Beam intensity required was $\sim 10^{11}$ protons/pulse for the first targeting arrangement and $\sim 5\times 10^{10}$ protons/pulse for the second. Increased efficiency of operation was achieved with dynamic intensity control provided by a pulsed parallel-plate electromagnetic separator operated with a 4-in. gap and 150 kV between the plates.[5] An appropriate signal from a preset scalar reading the output of counters directly before the entrance window of the bubble chamber triggered a spark gap across the spectrometer plates which discharged them in 2 μsec. The magnetic field remained and caused the beam to be deflected $\frac{3}{4}$ in. vertically, off the slit into the uranium collimator. In this way the usual variations in beam intensity due to statistical fluctuations and accelerator instability were largely eliminated. With a total beam in the channel of about 30 particles per pulse, the beam at the chamber was maintained constant to within two tracks per picture. Contamination from single-pion production in the target was small since the primary proton beam and the secondary protons from the target were set to differ little in momentum, while the secondary pions had considerably lower momentum. A measurement made in a similar beam[6] using a Čerenkov counter to distinguish pions from protons indicated a pion contamination of less than 0.1%. This was neglected as a source of background events in the analysis.

All the film has been scanned twice for events of interest. All events containing one or more charged or neutral decays were recorded and measured with conventional digitized measuring machines. Geometrical reconstruction and kinematical fitting of events with neutral V's were done with the use of the program PACKAGE. Of the three views measured, only the two chosen by the program to give maximum accuracy in determination of the dip angle of each track were used. Reconstruction and fitting of two prongs with charged decays was done with TVGP-SQUAW, which uses measurements in three views for reconstruction. The incident beam momentum was determined from measurements of noninteracting tracks and from well-identified examples of fits to elastic scattering. Both methods gave the same result. The observed width of the beam momentum distribution was consistent with that expected only from measurement error, approximately 1%. However, we assign $\pm 0.5\%$ uncertainty to the incident particle momentum for fitting purposes, allowing a rather larger spread than deduced from beam optics for effects such as scattering on slits and windows.

A total of 7200 events of two prongs and one neutral V, and 2500 of two prongs with the decay of either or both outgoing charged particles, candidates for events containing three final-state particles, were measured. Identity of the outgoing particles was established by the usual methods of requiring consistency of measured momenta with reaction kinematics and visually estimated bubble densities. The χ^2 for the kinematic fit was required to correspond to a probability level greater than 1%. In this way 1302 events with neutral V's were identified as examples of three-body channels (a), (b), and (c). Of these events, 45 were also consistent with four-body final states. They were assigned to the three-body category because the three-body fits are more constrained by the kinematical requirements. Similarly, all the ambiguities between $\Sigma^0 pK^+$ and ΛpK^+ were resolved in favor of the Λ since the fit with a Λ has four constraints and that with a Σ^0 only two. The decision in this case is greatly strengthened by appeal to the requirement that the angular distribution of any particle with respect to the incident beam direction be symmetrical about 90^0 in the center-of-mass system. In Fig. 2 we show the angular distribution of the proton produced with a hyperon and K^+ for the weighted total of 533 events with uniquely identified Λ's together with that including the 504 events with ambiguous identifi-

[4] C. Dols, University of California Radiation Laboratory Report No. UCRL-8346 (unpublished).

[5] UCRL Engineering Report EET-1071. This method of beam control was suggested by J. Murray. The pulsing gear was constructed under the supervision of R. Force. We are indebted to them for the success of the operation.

[6] We thank W. Wenzel for the use of equipment and aid in making this measurement.

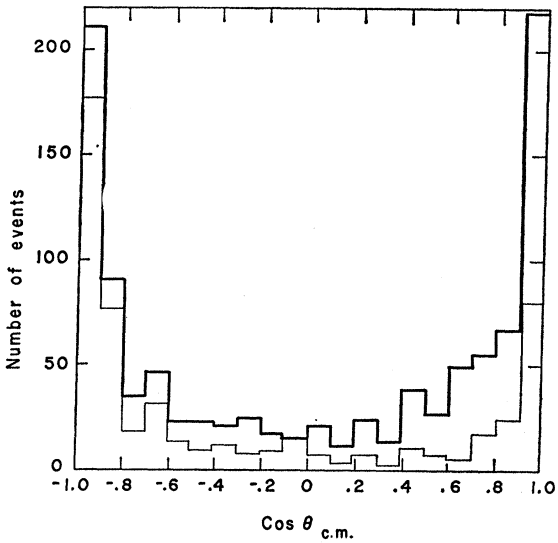

FIG. 2. Distributions of the cosine of the angle the final-state proton makes with the beam proton in the over-all center-of-mass system: light line, only unambiguously identified examples of the reaction $pp \rightarrow \Lambda pK^+$; heavy line, total sample of ΛpK^+, including events ambiguous between hypotheses $pp \rightarrow \Lambda pK^+$ and $pp \rightarrow \Sigma^0 pK^+$.

cation of the hyperon. Clearly the symmetry is improved if the events are combined. Thus, in all such cases of ambiguity the hyperon is considered to be a Λ. The angular distribution of the protons produced in unambiguous examples of the $\Sigma^0 pK^+$ final state is shown in Fig. 3. The distribution is not nearly as symmetric as that for ΛpK^+, reflecting the greater difficulty in resolving ambiguities with the two-constraint fit. The asymmetry is, however, in the same direction as that of the ambiguities which were assigned to ΛpK^+ and thus does not result from inclusion of misidentified Λ production events. We conclude that the source of this asymmetry is ambiguity with four-body hypotheses which have one constraint, and that the four-body background plus events lost due to misidentification amounts to about 10% of the sample, judging from the number of ambiguous events and the size of the production asymmetry.

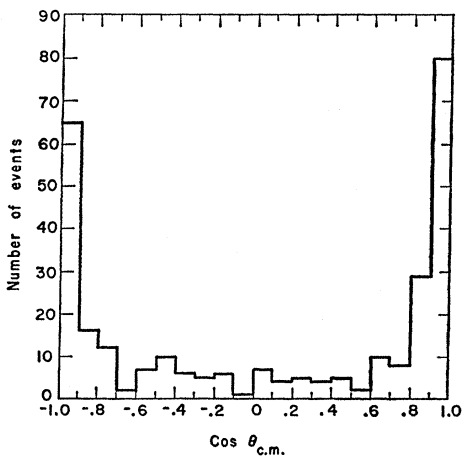

FIG. 3. Distribution of the cosine of the outgoing proton center-of-mass angle for unambiguously identified examples of the reaction $pp \rightarrow \Sigma^0 pK^+$.

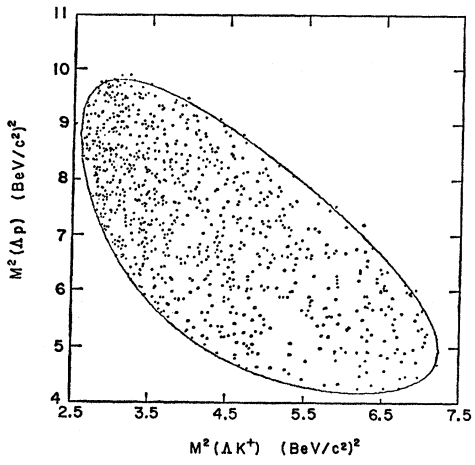

FIG. 4. Dalitz plot for reaction $pp \rightarrow \Lambda pK^+$.

Since the reaction (d) always yields an unobserved neutral product, kinematical constraints may be applied only if the Σ^+ momentum is known from measurement of the Σ^+ track and/or measurement of the decay product track. In either event, the momentum is generally poorly determined and kinematical ambiguities are more serious. Three kinds of ambiguities were present: Those involved in (i) distinguishing between Σ^+ decays and K^+ decays, (ii) distinguishing $\Sigma^+ nk^+$ from $\Sigma^+ pK^0$ with unobserved K^0 decay, and (iii) separating events with an additional, unobserved neutral. In fact, only an insignificant number of the first and second kinds appear, fitting to the decay kinematics and bubble-density estimates generally being sufficient to distinguish among the various hypotheses. Further, the ratio of observed numbers of $\Sigma^+ pK^0$ with K^0 decay to the number with unobserved K^0 decay, after correction for detection inefficiency and scanning biases, is 0.3 ± 0.1, indicating that the correct number of identifications of $\Sigma^+ pK^0$ events has been made. In the analysis of reaction (d) only the events consistent with $\Sigma^+ \rightarrow n\,\pi^+$ were used. This procedure is required since, to correct for scanning inefficiency, we impose a minimum projected decay angle cutoff of 10°. The decay angle of the proton from a Σ^+ with momentum greater than 1.4 BeV/c is necessarily smaller than 10°. We find that the corrected sample of data for reaction (d) is consistent with symmetry in the total center-of-mass frame and estimate from the number of ambiguities that contamination is $(5 \pm 2)\%$.

In these ways, ambiguities in identification were settled and events were assigned to particular categories. Table I gives the total number of observed events for each of the four reactions.

TABLE I. Event totals and cross sections for pp three-body reaction containing a K meson at 6 BeV/c.

Channel	Observed number	Corrected number	Cross section (μb)
Σ^+pK^+	916	1037	54_{-5}^{+3}
Σ^0pK^+	254	285	17_{-2}^{+4}
Σ^+pK^0			26 ± 4
$\Sigma^+\to\pi^+(n)$	87	113[b]	
$\Sigma^+\to p(\pi^0)$	45	56[b]	
$\Sigma^+p(K^0)$[a]			29 ± 5
$\Sigma^+\to\pi^+(n)$	84	126	
$\Sigma^+\to p(\pi^0)$	33		
$\Sigma^+K^+(n)$			57 ± 7
$\Sigma^+\to\pi^+(n)$	255	395	
$\Sigma^+\to p(\pi^0)$	72		

[a] Only half of the film was analyzed for the two-prong-with-decay topology.
[b] This number does not contain a correction for small-angle Σ^+ decays.

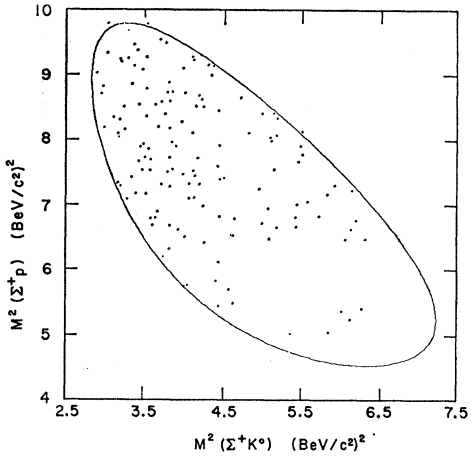

FIG. 6. Dalitz plot for reaction $pp\to\Sigma^+pK^0$.

III. PRODUCTION CROSS SECTIONS

Some fraction of events produced in the chamber escape detection in both scans. Corrections to the observed body of data, in addition to that due to ordinary scanning inefficiency, must then be made for inefficient detection of decays at small angles, decays at small and large distances from the production origin, as well as for undetected decays into neutral particles. Examination of the observed distributions of decays in time and angle permit estimates to be made of the detection efficiency. In addition, the requirement of a symmetric production angular distribution aids in determining detection biases. To correct for these inefficiencies, each event was weighted by the inverse of the probability for detection within a specified kinematic region. This region is determined by requiring events to be within a fiducial volume, to have decays with projected opening angles greater than 10° and less than 75°, and lengths greater than minima determined by particle identification: 1.5 cm for Λ's and K^0's, and 1.0 cm for Σ^+'s. The magnitude of these corrections may be inferred from the corrected numbers of events listed in Table I. The incident flux needed to compute the cross sections quoted in Table I was determined from a count of beam tracks in frames selected at regular intervals throughout the film. The scanning-measuring efficiencies were deduced from a comparison of processed events from the two scans and were found to be $80\pm3\%$ for scan I, $81\pm3\%$ for scan II. Errors quoted include statistical error in the number of events, an estimate of $\pm3\%$ error in flux determination, and estimated error $\pm5\%$ resulting from misidentifications and uncertainties in the magnitudes of the various corrections.

IV. ANALYSIS OF FINAL-STATE INTERACTIONS

The four states studied, ΛpK^+, Σ^0pK^+, Σ^+pK^0, and Σ^+nK^+, have similar properties in many respects. We will discuss them simultaneously as much as possible. Figures 4–7 are scatter plots of the squares of the effective masses of hyperon-nucleon versus hyperon-kaon systems. In each case a nonuniform density within the kinematic boundary of the Dalitz plot is

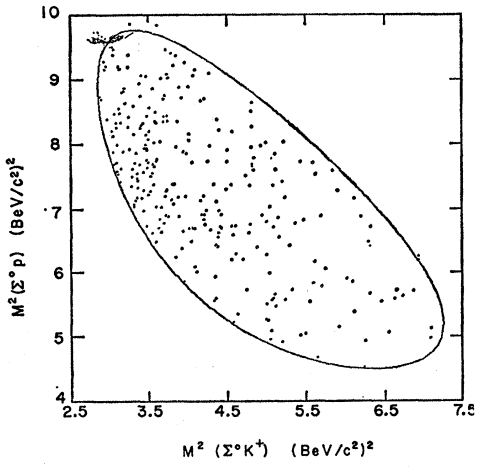

FIG. 5. Dalitz plot for reaction $pp\to\Sigma^0pK^+$.

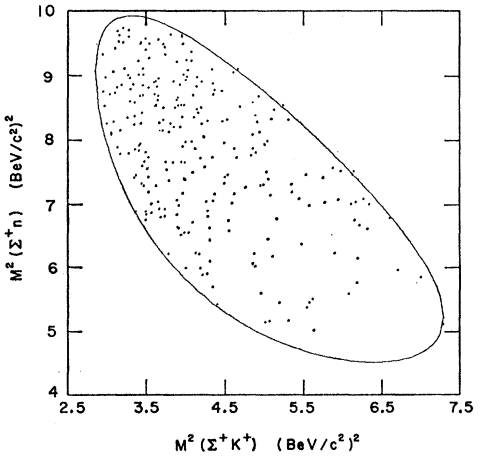

FIG. 7. Dalitz plot for reaction $pp\to\Sigma^+nK^+$.

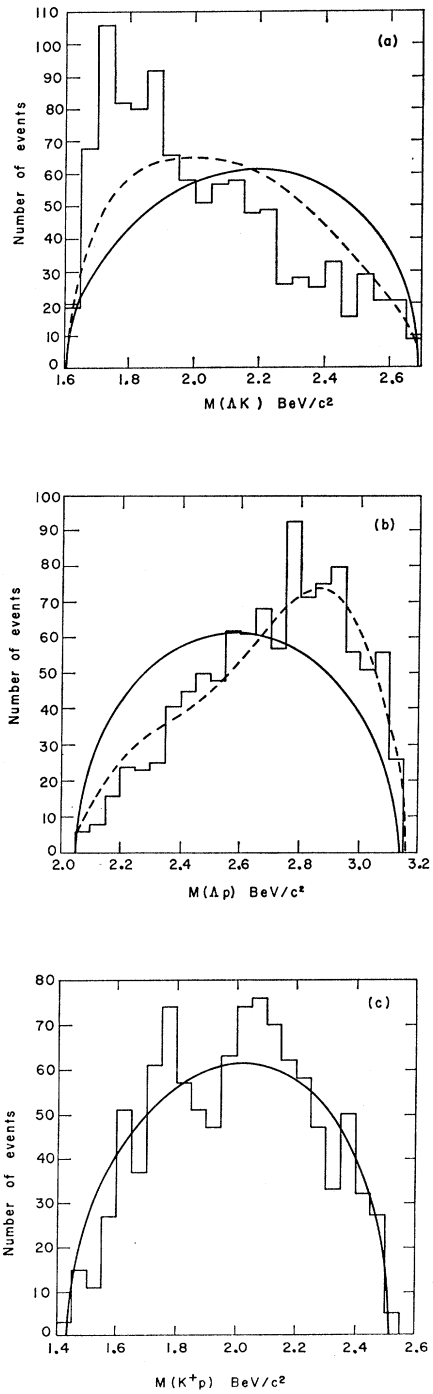

FIG. 8. Mass distributions in the channel ΛpK^+; (a) $M(\Lambda K^+)$, (b) $M(\Lambda p)$, (c) $M(K^+p)$. The solid curves are phase-space distributions while the dashed curves represent the effect of reflections, as discussed in the text.

apparent. A strong concentration of data points is noted at low values of Y-K mass, particularly in the ΛK^+ and Σ^+K^+ systems. In no case is there a clearly defined region in hyperon-nucleon effective mass within which the density of points is strikingly larger than in others. Rather, only in a region defined by limits on YK^+ effective mass is there such a concentration. The existence of only ΛK^+ and Σ^+K^+ final-state interaction is demonstrated more conclusively in the effective-mass distributions of Figs. 8–11, shown together with the corresponding phase-space distributions. Corrections to the data have been made here for observational biases, so that each observed event is weighted as discussed above. The bin heights in each histogram are the sums of the weights for individual events falling into the relevant bins. Statistical errors are given by the application of Poisson statistics to a weighted collection of events; thus, if

$$N=\sum_j w_j, \quad (\delta N)^2=\sum_j w_j^2.$$

The weights for reactions (a), (b), and (c) are relatively constant with average values 1.3, 1.3, and 1.6,

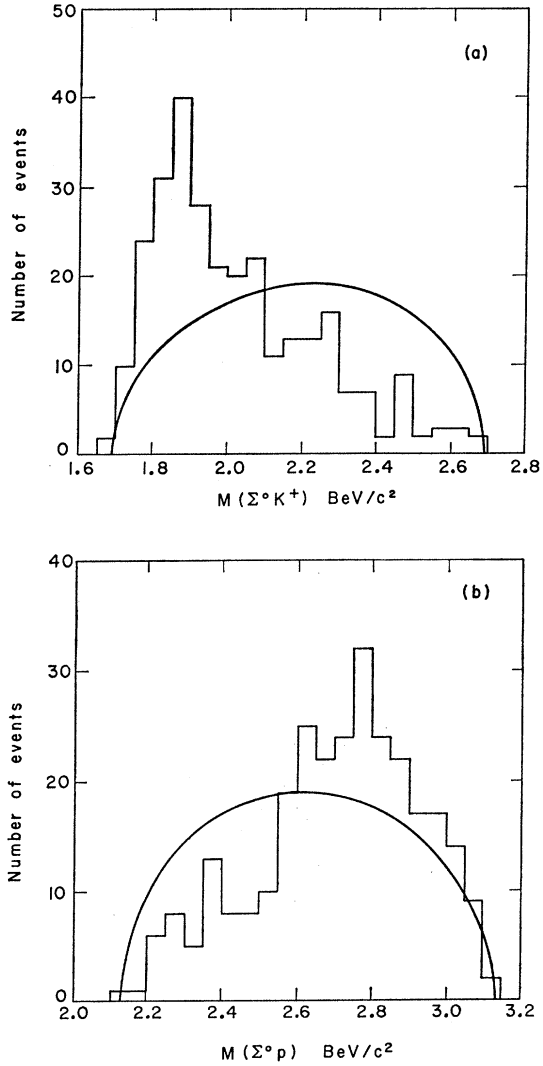

FIG. 9. Mass distributions in the channel Σ^0pK^+; (a) $M(\Sigma^0K^+)$, (b) $M(\Sigma^0p)$. The curves are phase-space distributions.

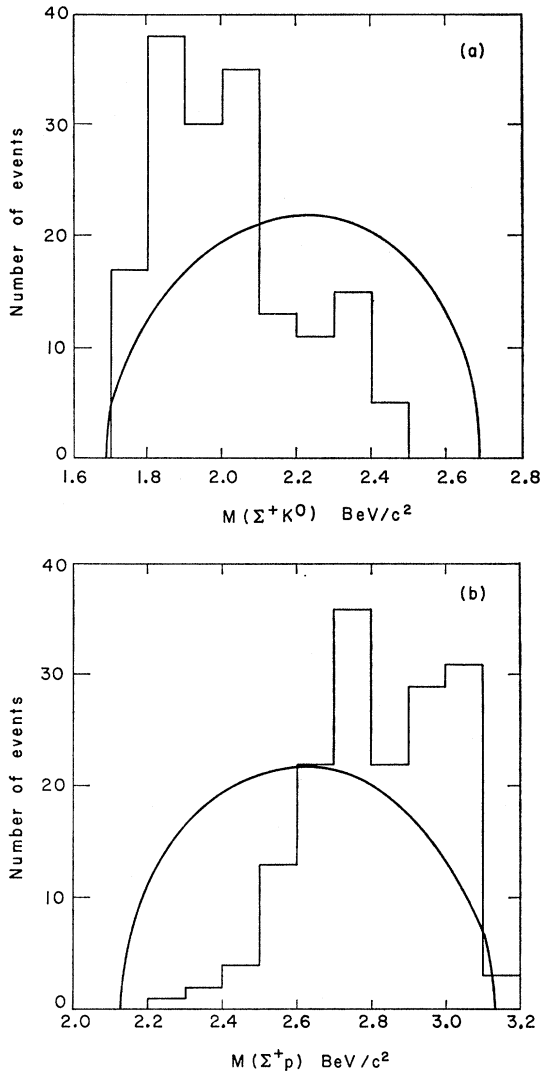

FIG. 10. Mass distributions in the channel Σ^+pK^0; (a) $M(\Sigma^+K^0)$, (b) $M(\Sigma^+p)$. The curves are phase-space distributions.

respectively. The weights for reaction (d) are distributed over a broad range with average value 2.6; consequently, error bars are displayed on the histograms of Figs. 11 and 20. In fact, none of the conclusions are substantially altered when unweighted distributions are considered. This is the case because only about 10% of the expected number of events with neutral V's, and 30% of the numbers with charged decays, are actually missing from the sample. In addition the detection inefficiencies are not strongly dependent on the momentum and angular distributions.

All the Y-N and Y-K mass distributions show considerable deviations from the statistical distribution, but most of the further discussion will be limited to the ΛpK^+ and Σ^+nK^+ states for a number of reasons. In the first state the hyperon-kaon system occurs only with isotopic spin $T=\frac{1}{2}$ and in the latter only with $T=\frac{3}{2}$, so that the analysis of resonance production is simplified. The Σ^0pK^+ and Σ^+pK^0 reactions appear qualitatively to have properties similar to those discussed below and the samples of these are severely limited statistically and probably more contaminated. Analysis of the latter reactions does not add to the conclusions about final-state interactions nor to the further elucidation of the production dynamics.

We have noted the nonuniformity in the Dalitz plot and the corresponding enhancements at low hyperon-kaon mass and high hyperon-nucleon mass. While it is not possible, in general, to demonstrate rigorously which of the two-body combinations are in resonance, we can nevertheless argue persuasively that the details of the nonuniformity are consistent with the production of only Y-K resonances. A simple check of this hypothesis consists of alternately assuming production

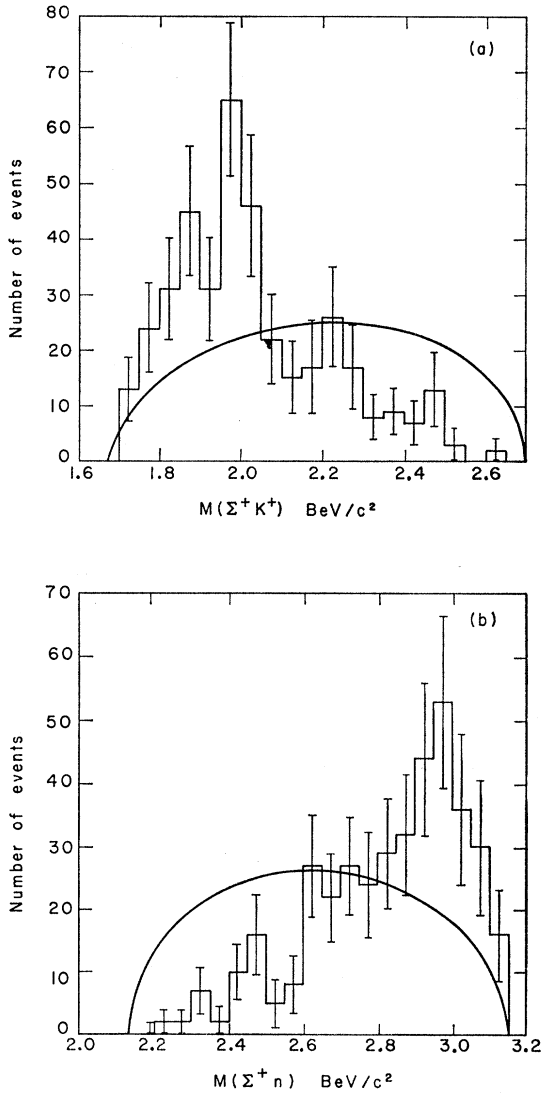

FIG. 11. Mass distributions in the channel Σ^+nK^+; (a) $M(\Sigma^+K^+)$, (b) $M(\Sigma^+p)$. The curves are phase-space distributions.

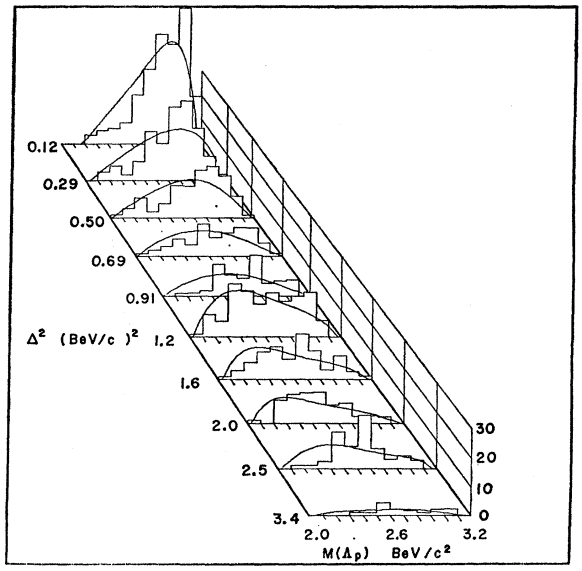

FIG. 12. The Λ-p mass distribution for the channel ΛpK^+ shown as a function of momentum transfer to the proton. The curves are phase-space distributions.

of the Y-K and Y-N systems with the observed mass distributions, followed by isotropic decay in their center-of-mass frames, and calculating the expected reflections in the Y-N and Y-K systems, respectively. The results of such calculations are shown in Fig. 8 for the ΛpK^+ reaction. It is clear that the Λp peak can be understood as a reflection of a ΛK^+ enhancement, while the converse does not hold.

The above assumption of an isotropic disintegration of the two-body system cannot be completely justified. The breakup angular distributions of either two-body system can be readily obtained from the Dalitz plots, Figs. 4–7. The ordinate and abscissa may be interpreted, respectively, as the square of the Y-nucleon mass and the cosine of the angle between the hyperon and the K line of flight in the Y-n center-of-mass system. The latter angle need not be isotropically distributed, as a consequence of the production mechanism, or final-state interactions. A new hyperon-nucleon resonance with a pathologically anisotropic decay distribution could be invoked to explain the over-all distribution in the Dalitz plot and the Y-K enhancement as a reflection. It is quite unnecessary to invoke such a new resonance with complicated properties, but we rather attribute the distribution purely to already well-established Y-K resonant interactions, specifically $N_{1/2}^*(1688)$ and $N_{3/2}^*(1920)$.

This conclusion is greatly reinforced by the observation that the Y-K production is predominantly peripheral and consistent with a single-pion-exchange model as discussed below. It should be noted that if those events produced with low momentum transfer to the initial proton are eliminated from the Λ-p mass distribution, a spectrum results that is in excellent agreement with phase space, as seen in Fig. 12. Thus, even in the region where peripheralism does not dominate, there is no suggestion of a dibaryon resonance. In calculating momentum transfer, there are, of course, two values for each event since the initial-state protons are indistinguishable. We use the smaller momentum transfer to define the identities of the initial-state protons when comparing with dynamical models and require our theoretical calculations to be consistent with this procedure. Such a choice is suggested by the strong peaks at low momentum transfer which characterize peripheral production. This procedure is well justified by the further demonstration below that the mechanism is indeed peripheral.

The Λp and ΛK^+ mass spectra may be understood to result from a quasi-two-body process, $pp \rightarrow N_{1/2}^* p$, proceeding via a peripheral mechanism, with subsequent decay of the N^* into ΛK^+. The conclusion that there is no evidence for a Λp resonant state is in agreement with that of Bierman *et al.*[7] The K^+p mass distribution for this reaction [Fig. 8(c)] shows structure not observed in K^+p elastic scattering with enhancements at 1.8 and 2.1 BeV/c^2. These features cannot be directly explained as reflections of the $N_{1/2}^*(1688)$ production. However, their absence in K^+p elastic scattering suggests that the peaks observed here are not resonances, but rather kinematical correlations associated with other aspects of the production process, or statistical fluctuations.

Consequently we conclude that we have observed no dibaryon resonances in either the $T=\frac{1}{2}$ or the $T=\frac{3}{2}$

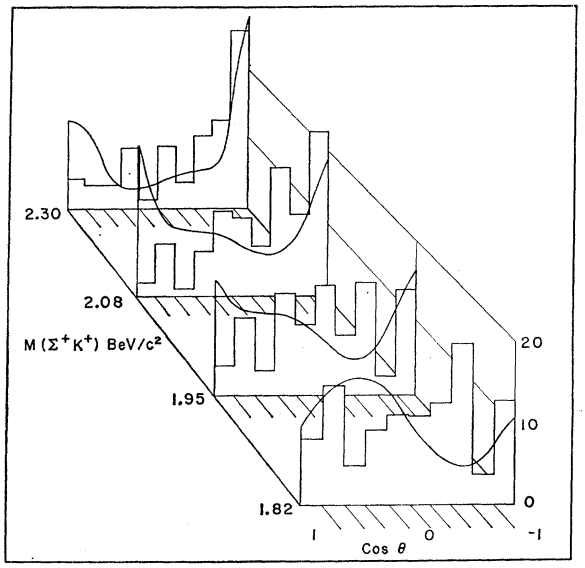

FIG. 13. Decay angular distribution of the Σ^+K^+ system produced in the channel Σ^+K^+n. The angle θ is between the Σ^+ and momentum transfer directions in the Σ^+K^+ rest system. The curves are predictions of pion exchange with a form factor.

[7] E. Bierman, A. P. Colleraine, and U. Nauenberg, Phys. Rev. 147, 922 (1966).

TABLE II. Pion-nucleon resonances between 1600 and 2000 MeV/c^2.[a]

N^*	Resonant state	M^0 (MeV)	Γ_{elastic} (MeV)	$\Gamma_{\text{inelastic}}$ (MeV)
$T=\frac{3}{2}$	$F_{7/2}$	1920	100	100
$T=\frac{1}{2}$	$S_{1/2}$	1700	216	24
	$D_{5/2}$	1670	56	84
	$F_{5/2}$	1688	72	38

[a] Values are quoted from Ref. 8.

state in the mass range from 2.05 to 3.14 BeV/c^2. It is conceivable that a dibaryon resonance in this range would be difficult to detect above the background of peripherally produced events in this reaction. Nevertheless, the absence of distinct localized enhancements in the hyperon-nucleon mass spectrum leads to the above conclusion. Further, we estimate that the cross section for the production of the enhancement reported by Melissinos *et al.*[3] is less than 0.2 μb in the present experiment.

V. NUCLEON ISOBAR PRODUCTION

Analyses of pion-nucleon elastic scattering have revealed evidence for the existence of three $T=\frac{1}{2}$ resonances near 1690 MeV and one $T=\frac{3}{2}$ resonance near 1920-MeV total c.m. energy.[8] The properties of these resonances inferred from the phase-shift analyses are listed in Table II. We interpret the observed resonance production as production of these π-nucleon resonances and their subsequent decay into hyperon and kaon.

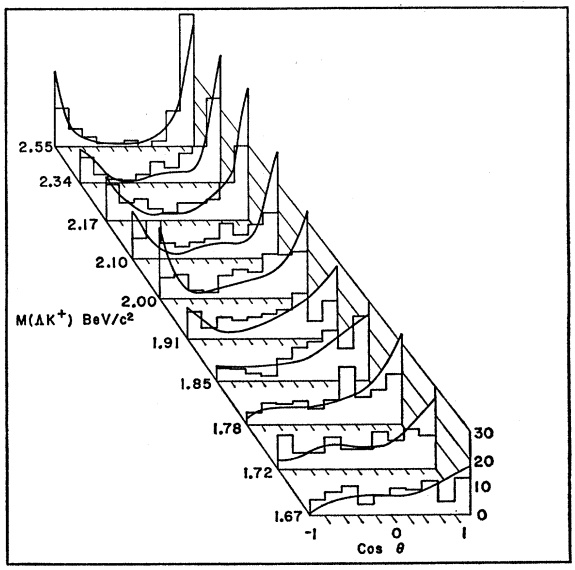

FIG. 14. Decay angular distribution of the ΛK^+ system. The angle θ is between the Λ and momentum-transfer directions in the ΛK^+ rest system. The curves are predictions of pion exchange with a form factor.

[8] A. H. Rosenfeld *et al.*, Rev. Mod. Phys. **39**, 1 (1967).

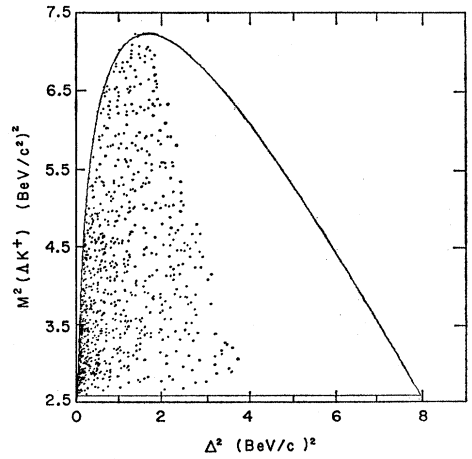

FIG. 15. Scatter plot of ΛK^+ mass versus momentum transfer for reaction $pp \to \Lambda K^+ p$.

Analysis of the angular and polarization distributions observed[9] in $\pi^+ p \to \Sigma^+ K^+$ show that this reaction proceeds in part through an $F_{7/2}$ resonance at 1925 MeV with width $\Gamma=175$ MeV, consistent with the parameters of the resonance observed in π-nucleon elastic scattering. The partial width of the $F_{7/2}$ into $\Sigma^+ K^+$ was found to be about 1 MeV. Our peak in the $\Sigma^+ K^+$ mass spectrum in the channel $\Sigma^+ n K^+$ is naturally interpreted as due to the production of this resonance and its subsequent decay into $\Sigma^+ K^+$. To estimate the rate of resonance production the distribution in Δ^2, momentum transfer to the neutron, and M, $\Sigma^+ K^+$ effective mass, were fitted to the expression

$$d^2\sigma = \frac{1}{(\alpha+\Delta^2)^2}\frac{q}{M} \times\left[1+c\frac{\Gamma_{\Sigma^+K^+}(M)}{(M_0{}^2-M^2)^2+M_0{}^2\Gamma^2}\frac{M^2}{q}\right]dM^2 d\Delta^2, \quad (1)$$

which is a sum of resonance and background contributions. The form factor $1/(\alpha+\Delta^2)^2$ is required to parameterize the strong peripheralism shown in the data. Here q is the momentum of the Σ^+ in the $\Sigma^+ K^+$ rest frame, M_0 the resonance energy quoted in Table II, Γ the total width, and c a number which characterizes the production cross section. The energy-dependent partial width into the channel $\Sigma^+ + K^+$ was taken to be

$$\Gamma_{\Sigma^+K^+} = \Gamma^0{}_{\Sigma^+K^+}\frac{(q/q_0)^{2l+1}(M_0/M)}{(q^2+X^2)^l/(q_0{}^2+X^2)^l}. \quad (2)$$

The "partial width" $\Gamma^0{}_{\Sigma^+K^+}$ is a measure of the coupling of the resonance to the decay channel in question, and the rest of the expression is the product of phase space, a barrier penetration factor, and form factor normalized to unity at the central mass M_0 of the resonance. Both these latter factors depend strongly on the orbital

[9] W. G. Holladay, Phys. Rev. **139B**, 1348 (1965).

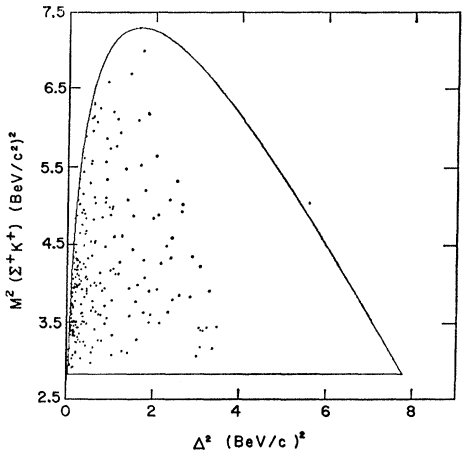

FIG. 16. Scatter plot of Σ^+K^+ mass versus momentum transfer for reaction $pp \to \Sigma^+nK^+$.

angular momentum l of the decay products. The X in the form factor is essentially the inverse of an effective range of interaction.[10]

The total width can be taken to be the sum of the energy-dependent partial widths for all decay modes. In principle, it is possible to determine both c and $\Gamma^0{}_{\Sigma^+K^+}$ by fitting. However, since the Σ^+K^+ partial width is very small compared to the total width, the shape of the distribution is insensitive to the partial width and only the product $c\Gamma^0{}_{\Sigma^+K^+}$ is determined. We take the total width to be that obtained from pi-nucleon scattering data and $c\Gamma^0{}_{\Sigma^+K^+}$ then determines the percentage of resonance production in this reaction. We find $(38\pm5)\%$ of the events result from resonance production and $(62\pm5)\%$ from background. The parameter α is found to be 0.35 ± 0.05 $(\mathrm{BeV}/c)^2$.

Determination of the rate of resonance production in the ΛpK^+ channel is rather more complicated. As mentioned above, there are three πp resonances near 1700 MeV. None of the branching ratios for decay into ΛK^+ is firmly known, nor have the relative production rates of these resonances been measured from non-strange particle production in p-p collisions. Some information about the parameters of these resonances has been obtained, however, from analysis of the differential cross section and Λ polarization in ΛK^0 production in $\pi^- p$ collisions.[11] Reasonable agreement results with a $J=\frac{5}{2}$ resonance with parity either positive or negative, total width $\sim$100 MeV and partial width into $\Lambda K^0 \sim$1–10 MeV. No analysis finds any evidence for the S-wave resonance in the ΛK^0 system. Appeal to the requirements of SU_3 symmetry to determine branching ratios of the $\frac{5}{2}^+$ and $\frac{5}{2}^-$ N^*'s is useless, since both resonances are thought to be members of octets and their partial widths are sensitive functions of their D/F ratios. For example, a D/F ratio of 3 forbids decay into ΛK. The study of baryon resonances[12] suggests that this ratio is often widely different in different N^* octets.

The data from this experiment are insufficient to determine the contributions of the various resonances. Since the associated production data suggest a large $J=\frac{5}{2}$ amplitude we fit the ΛK^+ mass spectrum to a single $F_{5/2}$ resonance at 1688 MeV together with a background contribution. As in the Σ^+nK^+ case, we fit to an expression corresponding to (1) and find $(54\pm6)\%$ of the events result from resonance production and $(46\pm6)\%$ from background. The fitted value for α is 0.53 ± 0.03 $(\mathrm{BeV}/c)^2$. Use of a $D_{5/2}$ resonance gives an equivalently good fit with comparable fraction of resonance production.

In principle, the angular distribution of the resonance decay products can provide the necessary information to determine the spin and parity of the parent state. In Fig. 13 we show the angular distribution, with respect to the momentum-transfer direction, of the hyperon in the Σ^+K^+ center-of-mass system and in Fig. 14 that for the ΛK^+. Predictions of a π-exchange model for production shown here with the experimental distributions will be discussed below. In both reactions the data in the resonance region are consistent with a resonance decay symmetric about 90° superimposed on a small amount of asymmetric background. The spin-density matrix of the resonance is not simply determined in proton-proton interactions, even for forward production. The possible angular distributions for high-spin resonances are rather complex and with the limited statistical accuracy of the data it is not possible to identify the contributing states.

VI. ONE-MESON-EXCHANGE MECHANISMS

As noted above the production angular distributions show the characteristic feature of peripheralism, a strong correlation between the final- and initial-state baryon directions. We display in Figs. 15 and 16 scatter

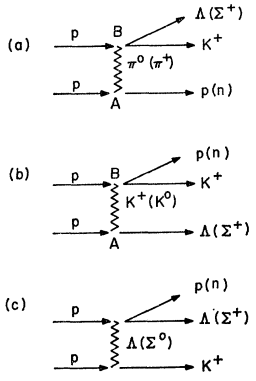

FIG. 17. The three single-particle-exchange diagrams applicable to the reactions $pp \to \Lambda pK^+$ and $pp \to \Sigma^+K^+n$. (a) pion exchange, (b) kaon exchange, and (c) baryon exchange.

[10] We take $X=350$ MeV, the fitted result obtained by S. L. Glashow and A. H. Rosenfeld, Phys. Rev. Letters **10**, 192 (1963).

[11] J. E. Rush and W. G. Holladay, Phys. Rev. **148**, 1444 (1966).

[12] R. D. Tripp, D. W. G. Leith, A. Minten, R. Armenteros, M. Ferro-Luzzi, R. Levi-Setti, H. Filthuth, V. Hepp, E. Kluge, H. Schneider, P. Barloutaud, P. Granet, J. Meyer, and J. P. Porte, Nucl. Phys. **B3**, 10 (1967).

plots of hyperon-kaon mass versus momentum transfer to the final-state nucleon, showing the high concentration of events at small momentum transfers. To determine the compatibility of the data with predictions of simple models for peripheral production, in particular one-particle-exchange processes, detailed comparisons have been made for the reactions $pp \to \Sigma^+K^+n$ and $pp \to \Lambda K^+p$.

It is clear that of the three lowest-order diagrams shown in Fig. 17, only the meson-exchange processes [17(a) and 17(b)] yield the observed characteristics. Calculations were made for the pion- and kaon-exchange models, using a Monte Carlo method to generate events distributed according to[13,14]

$$\frac{d^3\sigma}{dM^2 d\Delta^2 d\Omega} = \frac{1}{4\pi}\frac{G^2}{4\pi}\frac{1}{(2\bar{p}\bar{E})^2}\frac{\Delta^2+(m_p-m')^2}{(\Delta^2+\mu^2)^2}kM\frac{d\sigma(M)}{d\Omega}, \quad (3)$$

where

$$k=(1/M)[\tfrac{1}{4}M^4-\tfrac{1}{2}M^2(m_p^2+\mu^2)+\tfrac{1}{4}(m_p^2-\mu^2)^2]^{1/2}.$$

$\bar{p}$ and $\bar{E}$ are the center-of-mass momentum and energy of the incident proton; $G^2/4\pi$ = meson baryon-baryon coupling constant describing vertex A in Fig. 19; we use[15]

$$G^2_{pp\pi^0}/4\pi=15, \quad G^2_{p\Lambda K^+}/4\pi=15, \quad G^2_{p\Sigma^+K^0}/4\pi=0.64.$$

Δ^2 = four-momentum transfer squared to the recoil baryon m'; a nucleon for π exchange, Λ or Σ for K exchange;

μ = mass of exchanged meson, m_p = mass of proton;

M = invariant mass of the particles emerging at vertex B, e.g., ΛK^+ or Σ^+K^+ for π exchange;

$d\sigma(M)/d\Omega$ is the differential cross section for the two-body production at vertex B,[16] $\pi p \to YK$ or K-nucleon elastic or charge-exchange scattering;

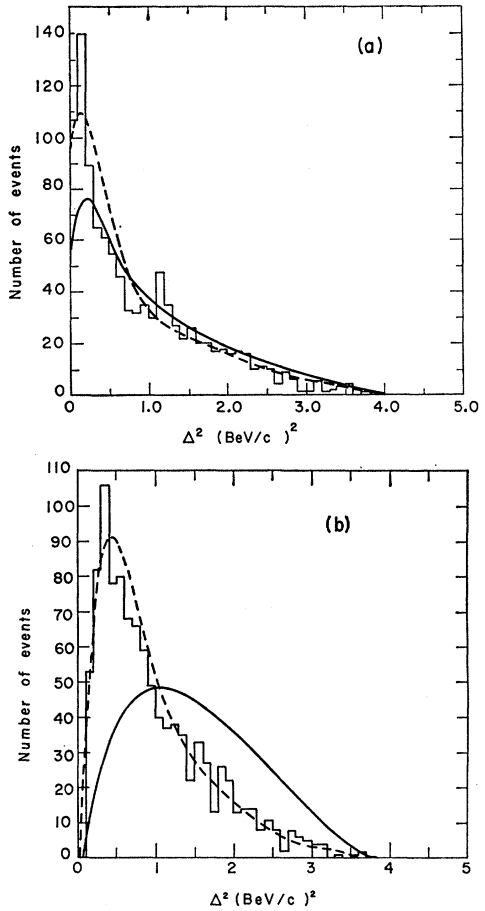

FIG. 18. (a) Distribution of momentum transfer to the final-state proton for reaction $pp \to \Lambda pK^+$. The dashed and solid curves are pion-exchange predictions with and without a form factor. (b) Distribution in momentum transfer to the Λ. The dashed and solid curves are K-exchange predictions with and without a form factor. The theoretical curves are normalized to the experimental histograms.

k is a kinematic factor which can be identified as the 3-momentum of the exchanged meson in the YK or NK center-of-mass frame consistent with actual two-body scattering at energy M.

The Monte Carlo technique provides great flexibility in the comparison of the theory with experiment. Any procedure applied to the actual data can be used on the events generated by the Monte Carlo program.

[13] G. F. Chew and F. A. Low, Phys. Rev. **113**, 1640 (1959); E. Ferrari, *ibid.* **120**, 988 (1960); F. Salzman and G. Salzman, *ibid.* **121**, 1541 (1961); T. Yao, *ibid.* **125**, 1048 (1962).

[14] J. D. Jackson and H. Pilkuhn, Nuovo Cimento **33**, 906 (1964); J. D. Jackson and J. T. Donahue, Phys. Rev. **139**, B428 (1965).

[15] J. K. Kim, Phys. Rev. Letters **19**, 1079 (1967).

[16] The meson-exchange calculations use data from the following references for associated production and K^+p elastic scattering.

K^+p elastic scattering: S. Goldhaber, W. Chinowsky, G. Goldhaber, Y. Lee, T. O'Halloran, T. F. Stubbs, G. M. Pjerrow, D. H. Stork, and H. K. Ticho, Phys. Rev. Letters **9**, 135 (1962); T. F. Stubbs, H. Bradner, W. Chinowsky, G. Goldhaber, S. Goldhaber, W. Slater, D. M. Stork, and H. K. Ticho, *ibid.* **7**, 188 (1961); C. Wohl (private communication); A. Bettini, M. Cresti, S. Limentani, L. Peruzzo, R. Santangelo, D. Locke, D. J. Crennel, W. T. Davies, and P. B. Jones, Phys. Letters **16**, 83 (1965); W. Chinowsky, G. Goldhaber, S. Goldhaber, T. O'Halloran, and B. Schwarzchild, Phys. Rev. **139B**, 1411 (1965); J. Debaisieux, F. Grard, J. Heughebaert, L. Pape, R. Windmolders, R. George, Y. Goldschmidt-Clermont, V. P. Henri, D. W. G. Leith, G. R. Lynch, F. Muller, I.-M. Perreau, G. Otter, and P. Sällström, Nuovo Cimento **43A**, 142 (1966); W. De Baere, J. Debaisieux, P. Dufour, F. Grard, J. Heughebaert, L. Pape, P. Peeters, F. Verbeure, R. Windmolders, R. George, Y. Goldschmidt-Clermont, V. P. Henri, B. Jongejans, D. W. G. Leith, A. Moisseev, F. Muller, J. M. Perreau, and V. Yarba, *ibid.* **45A**, 885 (1966).

$\pi^-p \to \Sigma^+K^+$: The data up to 1760 MeV/c are summarized by Holladay (Ref. 11); D. Berley and N. Gelfand, Phys. Rev. **139**, B1097 (1965); D. R. O. Morrison, CERN/TCL Physics 66-20 (unpublished).

$\pi^-p \to \Lambda K^+$: L. Bertanza, P. L. Connolly, B. B. Culwick, F. R. Eisler, T. Morris, R. Palmer, A. Prodell, and N. P. Samios, Phys. Rev. Letters **8**, 332 (1962); J. Keren, Phys. Rev. **133**, B457 (1964); J. A. Anderson, Ph.D. thesis University of California Radiation Laboratory Report No. UCRL-10838 (unpublished); F. Eisler, R. Plano, A. Prodell, N. Samios, M. Schwartz, J. Steinberger, P. Bassi, V. Borelli, G. Puppi, G. Tanaka, P. Woloscjek, V. Zobolli, M. Conversi, P. Franzini, I. Mannelli, R. Santangelo, and V. Silvestrini, Phys. Rev. **108**, 1353 (1957); O. I. Dahl, L. M. Hardy, R. I. Hess, J. Kirz, D. H. Miller, and J. A. Schwartz, *ibid.* **163**, 1430 (1967).

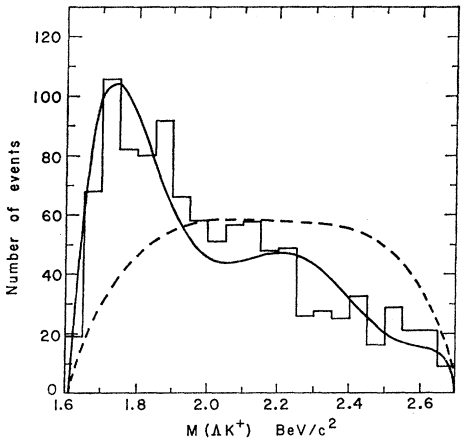

FIG. 19. ΛK^+ mass distributions for the reaction $pp \to \Lambda p K^+$. The solid curve is the pion-exchange prediction and the dashed curve that for K exchange. Both are normalized to the experimental histogram.

Thus we include the effect of selecting the smaller value of momentum transfer to define the event and any other relevant kinematic selections applied to the experimental distributions. In Fig. 18 we show the predictions of each model for the distribution in Δ^2, the momentum transfer to the recoil baryon. It is clear that in each case the experimental peak at small values is considerably narrower than that predicted. This feature of stronger damping at large momentum transfer has been demonstrated often in many peripheral processes.[14] Most other features of the data are reasonably consistent with a single-meson-exchange mechanism and the momentum-transfer discrepancy may be attributed to corrections to the model. In particular, absorption effects[14] due to competing inelastic channels, vertex form factors,[13] and off-mass-shell corrections are known to modify the Δ^2 dependence given by the propagator and vertex term in the simple single-particle-exchange process. Since the momentum-transfer distribution implies kinematic restrictions on the values other variables may assume, we include in further calculations a form factor $F(\Delta^2)$ multiplying the above expression (3). The functional form, chosen so that the modified expression reproduces the dependence of the data on Δ^2 is

$$F(\Delta^2)=\left(\frac{A-M_{\text{exch}}^2}{A+\Delta^2}\right)^2.$$

For the pion-exchange case the fitted values for A, in reactions (a) and (d) are, respectively, 5.0 and 1.8 $(\text{BeV}/c^2)^2$.

The most striking feature in either channel considered is the hyperon-kaon mass spectrum which must of course be reproduced by a relevant model. Predictions of both K exchange and π exchange are shown in Figs. 19 and 20. In both cases the π-exchange model satisfactorily reproduces the peaks in the ΛK^+ and Σ^+K^+ spectra while agreement with the K-exchange model is poor. The total cross sections calculated from the unmodified π-exchange mechanism are 96 and 414 μb for the $\Lambda p K^+$ and $\Sigma^+ K^+ n$ channels, respectively, while the unmodified K-exchange model gives 3.2 mb and 40 μb. Addition of the form factor reduces the π-exchange predictions to 60 and 130 μb, and the K-exchange predictions to approximately 320 and 5 μb. There is considerable uncertainty in the K-exchange predictions due to the inadequacy of a one-parameter form factor of the above form in this case. Both the modified and unmodified π-exchange predictions are in better agreement with the experimental data than the corresponding K-exchange predictions. As a further test of the model, we examine the Λ polarization obtained from the angular distribution of the decay products of

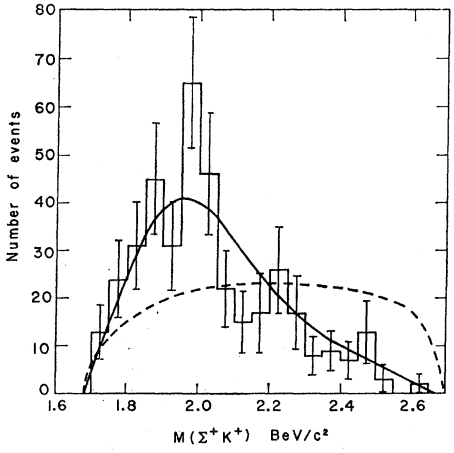

FIG. 20. Σ^+K^+ mass distribution for the reaction $pp \to \Sigma^+ n K^+$. The solid curve is the pion-exchange prediction and the dashed curve that for K exchange. Both are normalized to the experimental histogram.

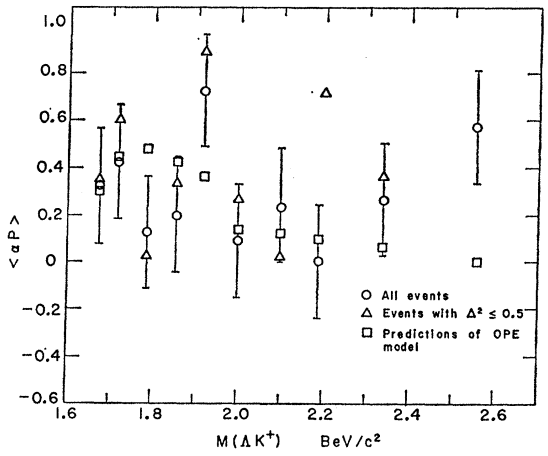

FIG. 21. Λ polarization for the reaction $pp \to \Lambda p K^+$ as a function of ΛK^+ mass. Polarizations for small-momentum-transfer events and pion-exchange predictions are shown.

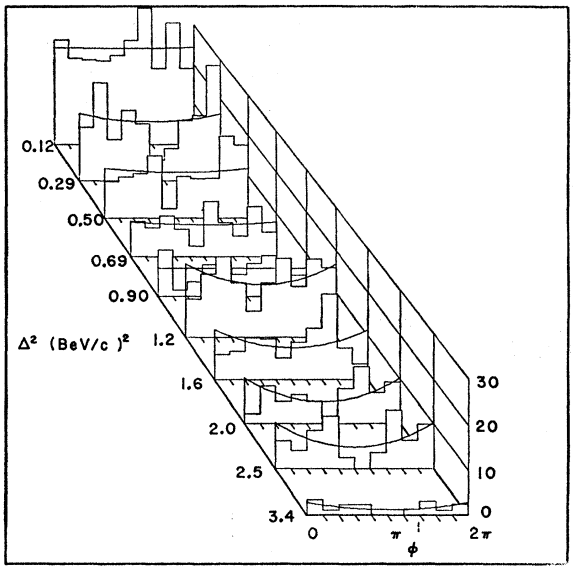

FIG. 22. Treiman-Yang distribution for the reaction $pp \rightarrow \Lambda pK^+$ as a function of momentum transfer. The small curves are predicted by pion exchange and are normalized to the experimental histograms.

the Λ in its rest frame. The polarization is measured along the normal to the plane containing the directions of the Λ and relevant initial proton in the ΛK^+ center-of-mass system. We show in Fig. 21 experimental values for the Λ polarization averaged over intervals in ΛK^+ mass, together with the predictions of pion exchange. Considerable polarization is noted, particularly at low momentum transfer and low ΛK^+ mass, in agreement with the results obtained for the associated production reaction $\pi^- p \rightarrow \Lambda K^0$. The K-exchange model predicts zero polarization since only a p-wave Λ-production amplitude is present. Thus we find the data consistent with that expected for a dominant pion-exchange mechanism with no evidence for a contribution from K exchange.

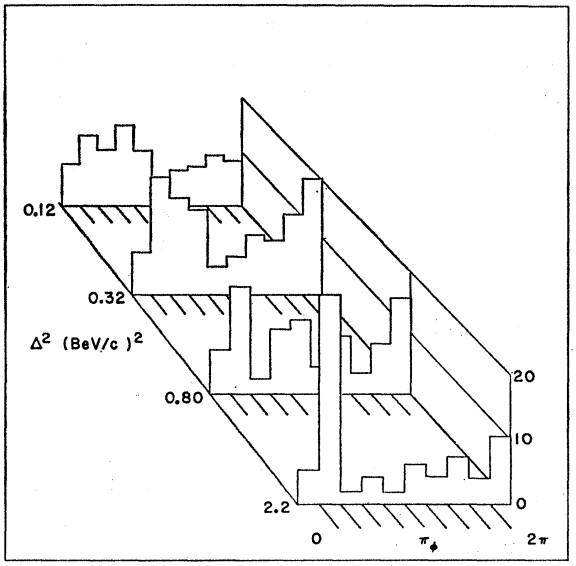

FIG. 23. Treiman-Yang angle distribution for the reaction $pp \rightarrow \Sigma^+ K^+ n$ as a function of momentum transfer.

We now study the predictions of the π-exchange model in more detail. Figures 13 and 14 show the angular distribution of the Σ^+ and Λ in the YK^+ center-of-mass system, with the momentum transfer as polar axis, together with the π-exchange predictions. Agreement is very satisfactory. In Figs. 22 and 23 we show the Treiman-Yang angle distributions and notice improved agreement with isotropy for events with small momentum transfer. Such substantially better agreement is to be expected in this region where the dominance of the pion-exchange contribution over other mechanisms is enhanced. Some deviation from isotropy may be expected to result from misidentification of the initial-state proton by selecting the lower momentum transfer. About 7% of the events with $\Delta^2 \leq 0.5(\text{BeV}/c)^2$ are in fact produced with large Δ^2, according to the distribution calculated with single-pion exchange, and their inclusion results from misidentification. The "calculated" distributions include this nonisotropy since they come from a Monte Carlo calculation as discussed.

We conclude that the single-pion-exchange mechanism with a form factor is in reasonable agreement with the data, particularly so at small momentum transfers. A more detailed analysis, involving absorbtive corrections, is necessary to determine if the discrepancies such as the sharp momentum-transfer peak and anisotropy in the Treiman-Yang angle distributions can be accommodated within a modified peripheral model. Unfortunately the complete lack of information about absorption in the final state makes such a calculation unfeasible.

VII. CONCLUSIONS

Three-body strange-particle states produced in proton-proton interactions proceed dominantly through the pion-exchange mechanism. There is considerable nucleon isobar production and these isobars, the $N_{3/2}^*(1920)$ and $N_{1/2}^*(1688)$, have properties consistent with those inferred from pion-nucleon scattering.

No evidence was found for the existence of a resonant hyperon-nucleon state with mass within the limits

$$2.05 \leq M_{\Lambda p} \leq 3.14 \text{ BeV}/c^2,$$
$$2.15 \leq M_{\Sigma^+ n} \leq 3.14 \text{ BeV}/c^2.$$

ACKNOWLEDGMENTS

Our particular thanks go to R. Watt and the bubble-chamber crew for careful attention to operations during a long, arduous, and sometimes excessively dull running period, with similar expressions of gratitude to the bevatron operating crew.

We thank Professor L. Alvarez for making the bubble chamber available. Professor E. Segrè provided valuable support and encouragement continuously and we express our gratitude to him.

W. Gage, B. Douglass, and Miss M. Corey contributed invaluably to the programming efforts and the scanning and measuring personnel contributed with their usual skill and industry.

PHYSICAL REVIEW VOLUME 165, NUMBER 5 25 JANUARY 1968

Measurements of the Polarization of Protons from Deuteron Photodisintegration*

F. F. Liu,† D. E. Lundquist,‡ and B. H. Wiik
High Energy Physics Laboratory, Stanford University, Stanford, California
(Received 20 September 1967)

The polarization of the proton produced by the photodisintegration of the deuteron has been measured at several angles for photon energies between 170 and 450 MeV. The polarization is found to be around −0.20 (Basel convention) for 90° c.m. and photon energies between 200 and 300 MeV. This is in reasonable agreement with a calculation by D. George based upon the Austern model. However, the calculation fails to explain the strong increase in polarization with increasing photon energies. At a photon energy of 450 MeV and 90° c.m. the proton polarization is as large as −0.60.

I. INTRODUCTION

PHOTODISINTEGRATION of the deuteron is the simplest reaction involving the interaction of a photon with a complex nucleus, and is therefore of theoretical interest.

In the energy range from threshold to about 100 MeV the reaction cross sections can largely be explained by the interaction of the photon with the two nucleons as they move in a static potential.[1] For photon energies above 100 MeV, the interaction of the photon with the meson current becomes increasingly important[2] so that the above theory is no longer sufficient. In the energy region from 100 to 1000 MeV the total and differential cross sections fall off smoothly with increasing energy, except for a pronounced peak near 250 MeV.[3–7] This peak has been qualitatively explained by assuming that the reaction proceeds through an intermediate state in which one of the nucleons is excited to the N^* isobar.[8,9]

Polarization measurements on the ejected protons determine the imaginary parts of partial-wave interference amplitudes. Hence, such measurements near 250 MeV provide a sensitive test to the model. Further measurements at higher energies can determine how far the model is still valid. Until now the proton polarization has been measured at only one point.[10] In this experiment, we have made a systematic study of the proton polarization between 170- and 450- MeV photon energies.

II. APPARATUS

The experimental arrangement is shown in Fig. 1. The momentum analyzed electron beam from the

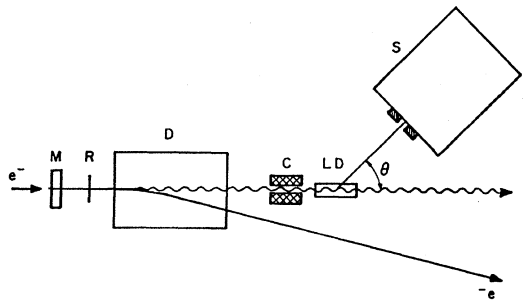

FIG. 1. The experimental layout. M, SEM beam monitor; R copper radiator; D, ditching magnet; C, lead collimator; LD liquid-deuterium target; S, 90° bend $n=0$ magnetic spectrometer.

* Work supported in part by the U. S. Office of Naval Research, Contract No. [Nonr 225(67)]. Distribution of this document is unlimited.

† Present address: Case Western Reserve University, Cleveland, Ohio.

‡ Present address: Argonne National Laboratory, Argonne, Ill.

[1] M. L. Rustgi, W. Zernik, G. Breit, and D. J. Andrews, Phys. Rev. **120**, 1881 (1960). W. Zickendraht, D. J. Andrews, M. L. Rustgi, W. Zernik, A. J. Torrnella, and G. Breit, *ibid.* **124**, 1538 (1961).

[2] G. R. Bishop and R. Wilson, in *Handbuch der Physik*, edited by S. Flügge (Springer-Verlag, Berlin, 1951), Vol. 42, pp. 309–361.

[3] E. A. Whalin, B. D. Schriever, and A. O. Hanson, Phys. Rev. **101**, 377 (1956).

[4] J. C. Keck, A. V. Tollestrup, Phys. Rev. **101**, 360 (1956).

[5] H. Myers, R. Gomez, D. Guinier, and A. V. Tollestrup, Phys. Rev. **121**, 630 (1961).

[6] R. Ching and C. Schaerf, Phys. Rev. **141**, 1320 (1965).

[7] R. Kose, W. Paul, K. Stockhorst, and K. H. Kissler, Z. Physik, **202**, 364 (1967).

[8] N. Austern, Phys. Rev. **100**, 1522 (1955).

[9] F. Zachariasen, Phys. Rev. **101**, 371 (1956).

[10] F. J. Loeffler, T. R. Palfrey, Jr., and T. O. White, Jr., Phys. Rev. **131**, 1844 (1963).